PETROPHYSICS, VOL. 44, NO. 3 (MAY-JUNE 2003); P. 196–204, 9 FIGURES

Apparent Resistivity Correction for Tensor Induction Well Logging in a Deviated Well in an Anisotropic Medium

Ertan Peksen[1] and Michael S. Zhdanov[1]

ABSTRACT

In this paper we study the principles of tensor induction well logging (TIWL) in a deviated well in an anisotropic medium. We examine the theoretical formulae for the tensor apparent conductivities of the transverse anisotropic medium, developed for an ideal tensor induction instrument with coinciding positions of three mutually orthogonal transmitters at one point and all three receivers at the other point in a borehole. We demonstrate that these formulae can be corrected for practical instrument design, where, due to technical reasons, transmitter coils with different orientations are spatially separated and receiver coils are spatially separated as well. We introduce the corrected formulae for a practical TIWL instrument. The numerical study shows that, for different deviation angles and for different anisotropy values, the corrected apparent conductivities are practically the same as the theoretical apparent parameters.

INTRODUCTION

Induction well logging in anisotropic formations has recently become an area of active research and industrial development. Kriegshauser et al. (2000a, b) described the new induction instrument comprising three mutually orthogonal transmitter coils and similar receiver coils. A number of papers discussing multi-component induction logging appeared at the 42nd meeting of the SPWLA in Houston, (Cheryauka and Zhdanov, 2001b; Kriegshauser et al., 2001a; Martin et al., 2001; Zhang et al., 2001; Zhdanov et al., 2001b) and at the 71st meetings of SEG in San Antonio, in 2001 (Cheryauka and Zhdanov, 2001c; Yu et al., 2001; Kriegsauser et al., 2001b; Lu and Alumbaugh, 2001; Zhang, 2001; Zhang and Mezzatessa, 2001).

The response of the tri-axial induction instrument is formed by three components of the magnetic field due to each of three transmitters, thus forming a tensor array of nine signals, which we call an *induction tensor*. This tensor is determined by the conductivity tensor of the medium. The goal of interpretation is to recover the conductivity tensor from the observed data. The foundations of tensor induction well logging (TIWL) in anisotropic formations were outlined in the paper by Zhdanov, Kennedy, and Peksen (2001a), where the authors derived the expressions for an apparent conductivity tensor based on the low frequency asymptotic of the induction tensor. These formulae were derived only for an ideal instrument that comprises three mutually orthogonal transmitter coils located at the same point and similar receiver coils located at another point. In practice, however, it is technically difficult to place all three transmitter coils at one point, or to place all three receiver coils at one point. That is why, in the practical instrument (for example, in the 3DEX instrument developed by Baker Atlas), the transmitter coils with different orientations are located at some distance from one to the other (Figure 1). A similar design is used for the receiver coils. In this situation the theoretical formulae derived in Zhdanov et al., (2001a, b) for apparent horizontal and vertical conductivities may produce an erroneous result.

In this work, we develop a method of apparent conductivity correction to analyze practical induction instrument data. Throughout this paper, we call our hypothetical instrument the "ideal instrument" and the typical design of the industrial instrument the "practical instrument." Using numerical

Manuscript received by the Editor March 28, 2002; revised manuscript received December 17, 2002.
[1]University of Utah, Department of Geology and Geophysics, Salt Lake City, UT USA

simulation, we demonstrate that the correction method introduced in this paper improves the accuracy of the evaluation of the anisotropic parameters of the medium by using the practical tri-axial induction data.

CALCULATION OF THE APPARENT CONDUCTIVITIES IN TENSOR INDUCTION WELL LOGGING

The ideal tensor induction well logging instrument detects three components of the magnetic field due to each of three transmitters for a total of nine signals, which form the magnetic induction tensor

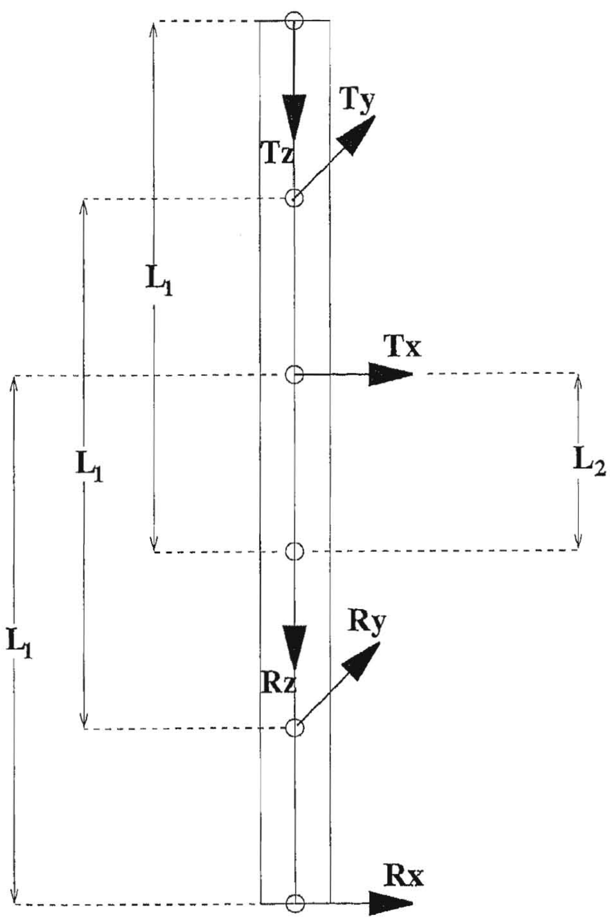

FIG. 1 A simplified practical instrument has three mutually ortogonal transmitters and three receivers as an ideal instrument does, but they are separated from each other.

$$\hat{\mathbf{H}} = \begin{bmatrix} H_x^x & H_x^y & H_x^z \\ H_y^x & H_y^y & H_y^z \\ H_z^x & H_z^y & H_z^z \end{bmatrix}, \qquad (1)$$

where superscripts refer to the transmitter components and subscripts refer to the receiver components.

In the Cartesian system of coordinates (x,y,z), with the axis z directed along the axis of symmetry of the transversely isotropic (TI) conductive medium, the conductivity tensor can be represented by

$$\hat{\sigma} = \begin{bmatrix} \sigma_h & 0 & 0 \\ 0 & \sigma_h & 0 \\ 0 & 0 & \sigma_v \end{bmatrix},$$

where σ_h is the horizontal conductivity and σ_v is the vertical conductivity. The magnetic field components are given in formula (1) in a coordinate system defined by the horizontal and vertical principal axes of the conductivity tensor. In practice, the orientation of the transmitter and receiver coils will be arbitrary with respect to this coordinate system. In order to use the representation of the field tensor $\hat{\mathbf{H}}$ for an instrument having an arbitrary orientation with respect to the principal axes of the conductivity tensor, it is necessary to transform the transmitter moment in the instrument frame (denoted by (x', y', z')) into the medium coordinates (denoted by (x,y,z)). This transformation can be made by application of the rotational matrix $\hat{\mathbf{R}}$ (Moran and Gianzero, 1979; Zhdanov et al., 2001a). The rotation matrix $\hat{\mathbf{R}}$ consists of two rotations

$$\hat{\mathbf{R}} = \hat{\mathbf{R}}_\beta \hat{\mathbf{R}}_\alpha,$$

where $\hat{\mathbf{R}}_\alpha$ describes the rotation around y'

$$\hat{\mathbf{R}}_\alpha = \begin{bmatrix} \cos\alpha & 0 & -\sin\alpha \\ 0 & 1 & 0 \\ \sin\alpha & 0 & \cos\alpha \end{bmatrix},$$

and $\hat{\mathbf{R}}_\beta$ describes the rotation around the z $(=z')$ axis through an angle β, and

$$\hat{\mathbf{R}}_\beta = \begin{bmatrix} \cos\beta & \sin\beta & 0 \\ -\sin\beta & \cos\beta & 0 \\ 0 & 0 & 1 \end{bmatrix},$$

where α represents the relative deviation angle between the instrument axis and the "vertical" principal axis of the conductivity tensor, and β represents the rotation of the instrument on it own axis.

The product of these two rotation matrices is given by

$$\hat{\mathbf{R}} = \hat{\mathbf{R}}_\beta \hat{\mathbf{R}}_\alpha = \begin{bmatrix} \cos\alpha\cos\beta & \sin\beta & -\sin\alpha\cos\beta \\ -\cos\alpha\sin\beta & \cos\beta & \sin\alpha\sin\beta \\ \sin\alpha & 0 & \cos\alpha \end{bmatrix}. \quad (2)$$

The matrix of the magnetic induction tensor in the instrument frame is related to the matrix of the magnetic induction tensor in the medium coordinate frame by the following formula:

$$\hat{\mathbf{H}}' \equiv \hat{\mathbf{R}}\hat{\mathbf{H}}\hat{\mathbf{R}}^{-1} = \hat{\mathbf{R}}\hat{\mathbf{H}}\hat{\mathbf{R}}^{\mathrm{T}} . \quad (3)$$

The components of $\hat{\mathbf{H}}'$ are used in the estimation of receiver voltages.

Appendix derives a low-frequency approximation for the tensor induction magnetic field components and gives formulas for the apparent horizontal and vertical conductivities, σ_{ha}^T and σ_{ha}^T, the apparent anisotropy coefficient, λ_{ha}^T, and the apparent relative deviation angle, α_a^T, for the ideal instrument.

APPARENT CONDUCTIVITIES FOR THE PRACTICAL INSTRUMENT

A simplified design of a typical practical instrument is shown in Figure 1. For this instrument, all three transmitter coils and all three receiver coils are placed at different points along the sonde axis. However, the distances between the transmitter and receiver coils with the same orientations are the same, L_1, while the distances between cross oriented transmitters and receivers are different (see Figure 1). For example, the distance between the x-oriented transmitter dipole and the z-oriented receiver dipole is $L_2 \neq L_1$. The analysis of formulae (A.6), (A.7), (A.8), and (A.9) shows that the expressions for apparent parameters (horizontal and vertical conductivities, anisotropy coefficient, and relative deviation angle) contain only four components of the magnetic induction tensor: $H_{x'}^{x'}$, $H_{y'}^{y'}$, $H_{z'}^{z'}$, and $H_{z'}^{x'}$. We should recall now that these formulae were derived in a homogeneous TI medium. It is clear that in a homogeneous TI medium the components depend only on the distance between the transmitter and receiver, and they do not depend on the relative locations of the transmitters along the sonde axis. Therefore, the components, $H_{x'}^{x'}$, $H_{y'}^{y'}$, and $H_{z'}^{z'}$ are the same for the ideal and practical instruments.

At the same time, the $H_{z'}^{x'}$ component is different for the ideal and practical instruments, because the distance L_1 between the x-oriented transmitter dipole and the z-oriented receiver dipole for the ideal instrument is different than the distance L_2 for the practical instrument. However, from formula (A.3) we see that the $H_{z'}^{x'}$ component is inversely proportional to the transmitter-receiver separation. As a result, we have

$$\left(\Im H_{z'}^{x'}\right)_{L_1} = \left(\Im H_{z'}^{x'}\right)_{L_2} \frac{L_2}{L_1}, \quad (4)$$

where $(\Im H_{z'}^{x'})_{L_1L_2}$ is the imaginary magnetic field component with the transmitter-receiver separation equal to L_1 or L_2, respectively.

Thus, we can use theoretical formulae (A.6), (A.7), (A.8), and (A.9)for computing the apparent parameters for the practical instrument data, if we replace $(\Im H_{z'}^{x'})_{L1}$ with the expression $(\Im H_{z'}^{x'})_{L2}(L_2/L_1)$ according to equation (2). The new corrected formulae for the apparent parameters computed for the practical instrument are

$$\sigma_{ha}^c = \frac{1}{2g_0}\left[(\Im H_{x'}^{x'})_{L_1} + \frac{1}{2}(\Im H_{z'}^{z'})_{L_1} + \sqrt{\left((\Im H_{x'}^{x'})_{L_1} - \frac{1}{2}(\Im H_{z'}^{z'})_{L_1} \right)^2 + 2(\Im^2 H_{z'}^{x'})_{L_2}\left(\frac{L_2}{L_1}\right)^2} \right], \quad (5)$$

$$\alpha_a^c = \frac{1}{2}\sin^{-1}\left[\frac{2(\Im H_{z'}^{x'})_{L_2}(L_2/L_1)}{(\Im H_{x'}^{x'})_{L_1} + (\Im H_{z'}^{z'})_{L_1} - 3g_0\sigma_{ha}^c} \right], \quad (6)$$

where σ_{ha}^c is the corrected horizontal apparent conductivity, and α_a^c is the corrected apparent relative deviation angle. The subscripts L_1 and L_2 correspond to transmitter-receiver distances and indicate that the magnetic field is measured or calculated at these distances. Equation (A.7) does not need to be modified since this formula does not contain the $H_{z'}^{x'}$ component. Once the horizontal apparent conductivity is calculated, the vertical conductivity may be obtained from equation (A.9):

$$\sigma_{va}^c = \frac{\sigma_{ha}^c}{(\lambda_a^c)^2}. \quad (7)$$

NUMERICAL EXAMPLES

In this section we examine the accuracy of the corrected formulae for the apparent parameters, using numerical simulation. For simplicity, we consider the transverse anisotropic model of the rock formation without borehole and invaded zones. We do not include the borehole effect in the modeling study since the borehole correction is usually performed for induction tool data before any other interpretation.

The distances between the transmitter positions and the receiver positions in the practical instrument are $L_1 = 1.0$ m and $L_2 = 0.40$ m. The operating frequency range is up to 30 kHz. The model parameters are the horizontal resistivity 10 ohm-m, the vertical resistivity 160 ohm-m, and the anisotropy coefficient is 4. The relative deviation angles are selected equal to 10° and 30°.

We computed the synthetic data for ideal and practical induction instruments, and applied the corrected formulae (5) and (7) to the synthetic data obtained for the practical instrument with the relative deviation angle $\alpha = 10°$. Figure 2 presents the results of computing the horizontal apparent resistivity curves for the ideal instrument (solid lines) and for the practical instrument (dashed lines). The bottom part of Figure 2 shows the comparison of the apparent resistivities calculated for the ideal and practical instruments without a correction factor (by using formula (A.6), while the top part presents the same results obtained for the practical instrument with the corrected formula (5). One can see that, after correction, two apparent resistivity curves generated for the ideal (solid line) and practical (dashed line) instrument responses are almost identical. The vertical apparent resistivity curves for the instruments with the relative deviation angle $\alpha = 10°$ are given in Figure 3. Note that the vertical apparent resistivity curve computed for the practical instrument data by the theoretical formula derived for the ideal instrument becomes negative (dashed line in Figure 3, bottom panel), while after the correction we obtain reasonable values for the vertical apparent conductivity (dashed line in Figure 3, top panel), coinciding with the curve for the ideal instrument (solid line). Figures 4 and 5 display similar results for the ideal and practical instruments with the relative deviation angle $\alpha = 30°$. In this case, we correct our practical instrument data very well for the horizontal apparent resistivity and relatively well for the vertical resistivity. The corrected apparent vertical resistivity for the practical and ideal instruments diverge slightly with the increase of the frequency (Figure 5, top panel).

In the next set of numerical experiments we investigate the behavior of the apparent resistivity curves in the layered anisotropic formations. The distance between the transmitter's position and the receiver's position is 1.0 m for the ideal instrument, and the transmitter-receiver separations for the practical instrument, shown in Figure 1, are as follows: $L_1 = 1.0$ m and $L_2 = 0.40$ m. The calculations are performed for an instrument moving along the borehole

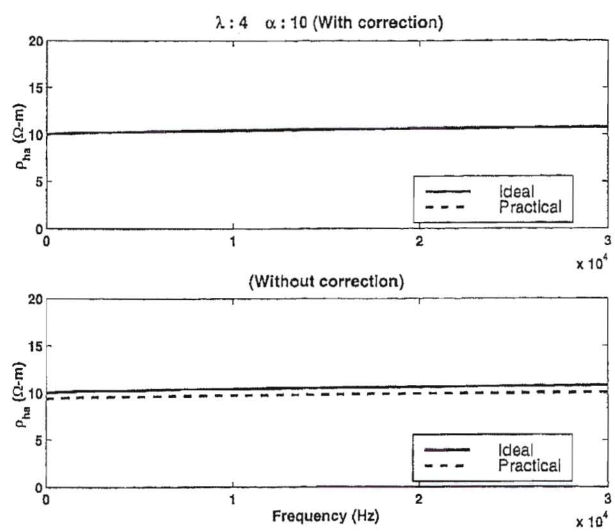

FIG. 2 An anisotropic model with the horizontal resistivity 10 ohm-m and the vertical resistivity 160 ohm-m. The relative deviation angle is 10°. Panels show horizontal apparent resistivity curves for the ideal instrument (solid lines) and for the practical instrument (dashed lines). The bottom panel shows the comparison of the apparent resistivities calculated for the ideal and practical instruments without a correction, while the top panel presents the same results obtained for the practical instrument with the correction.

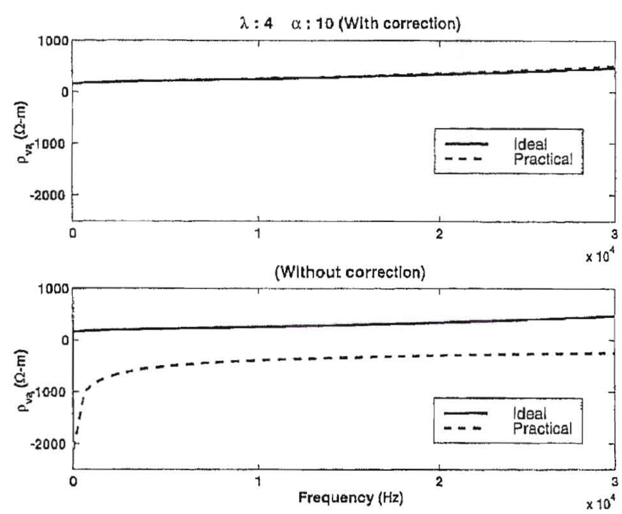

FIG. 3 An anisotropic model with the horizontal resistivity 10 ohm-m and the vertical resistivity 160 ohm-m. The relative deviation angle is 10°. Panels show vertical apparent resistivity curves for the ideal instrument (solid lines) and for the practical instrument (dashed lines). The bottom panel shows the comparison of the apparent resistivities calculated for the ideal and practical instruments without a correction, while the top panel presents the same results obtained for the practical instrument with the correction.

upward with measurements every 0.25 m. The operating frequency is 20 kHz.

The synthetic data were computed using the GT3D code developed by the Consortium for Electromagnetic Modeling and Inversion (CEMI) at the University of Utah (Cheryauka and Zhdanov, 2001a). The response of the layered anisotropic model was calculated in the model coordinate system. The result then was transformed from the model frame to the instrument frame, using equation (3).

We assume that tensor induction logging is conducted by an instrument oriented along the borehole so that the "vertical" transmitter and receiver are oriented along the borehole. We calculate the model responses (induction tensor components for the ideal and practical instruments) for the different parameters of the layered anisotropic models. Using these responses as the synthetic observed data, we compute the low frequency (σ^T_{ha} and σ^T_{va}) apparent conductivities according to the theoretical formulae (A.6) and (A.9) for the ideal instrument. The apparent conductivities, σ^T_{ha} and σ^T_{va}, for the practical instrument are computed using the corrected formulae (5) and (7) as they are described in the previous section. The results are plotted as apparent resistivity curves, ρ^T_{ha}, ρ^T_{va}, ρ^c_{ha}, and ρ^c_{va}, versus depth for a different relative deviation angle α, equal to 30° and 60°, respectively (Figures 6 through 9).

Each of the Figures 6 and 7 has three panels. The first panel on the left shows the parameters of the layered model. The second two panels present the apparent resistivity curves versus depth. The bold solid lines show the true parameters of the model. The apparent resistivities ρ^T_{ha} and ρ^T_{va} obtained by the theoretical formulae for the ideal instrument are shown by the bold solid-dotted lines. The black solid-dotted lines represent the apparent resistivities computed for the practical instrument by the theoretical formulae (A.6) and (A.9) without correction. The gray solid-dotted lines show the same parameters computed for the practical instrument data after corrections. Solid lines describe the positive values of the apparent resistivities, while the dotted lines correspond to the negative values.

The data were contaminated by 3% random Gaussian noise at each transmitter-receiver position. Note that, for a vertically oriented instrument, there is no need for correction because the induction tensor component $H_z^{x'}$ is equal to zero. In a deviated borehole we observe significant differences between the bold solid-dotted and gray solid dotted lines, which correspond to the apparent resistivities computed without and with the correction. As a rule, after the correction the apparent resistivities computed for the practical instrument coincide with the theoretical apparent resistivities for the ideal instrument. Thus, we can conclude that

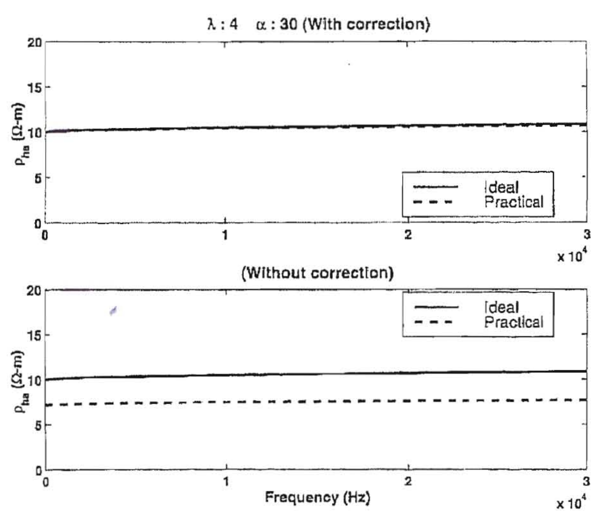

FIG. 4 An anisotropic model with the horizontal resistivity 10 ohm-m and the vertical resistivity 160 ohm-m. The relative deviation angle is 30°. Panels show horizontal apparent resistivity curves for the ideal instrument (solid lines) and for the practical instrument (dashed lines). The bottom panel shows the comparison of the apparent resistivities calculated for the ideal and practical instruments without a correction, while the top panel presents the same results obtained for the practical instrument with the correction.

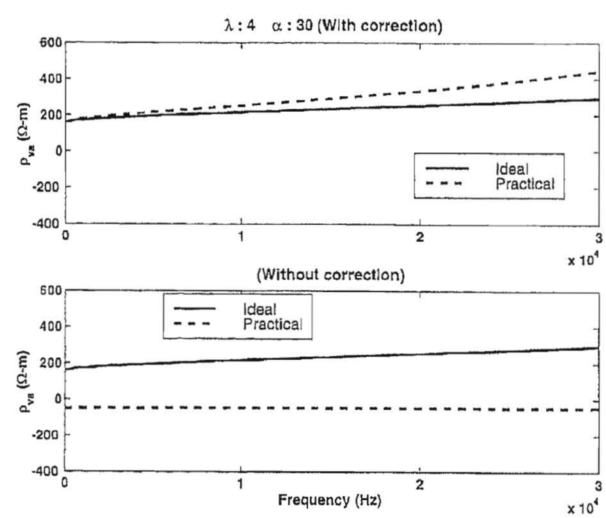

FIG. 5 An anisotropic model with the horizontal resistivity 10 ohm-m and the vertical resistivity 160 ohm-m. The relative deviation angle is 30°. Panels show vertical apparent resistivity curves for the ideal instrument (solid lines) and for the practical instrument (dashed lines). The bottom panel shows the comparison of the apparent resistivities calculated for the ideal and practical instruments without a correction, while the top panel presents the same results obtained for the practical instrument with the correction.

the corrected formulae work extremely well for all these models.

We also considered a multi-layered model of anisotropic formations, based on the known benchmark "Chirp" model (Fang and Wang, 2000). This model is represented by the black solid line in the left panel of Figure 8 (the horizontal resistivity profile). We modified this model, adding a profile of vertical resistivity (right panel in Figure 8). The results of the synthetic TIWL data interpretation for different relative deviation angles 30° and 60° are shown in Figures 8 and 9. Once again the apparent resistivities describe well the horizontal resistivity and recover relatively well the vertical resistivity. These results show that, in the case of complicated geoelectrical models, the simple interpretation tool based on apparent resistivity can be used.

CONCLUSION

In this paper we have demonstrated that the theoretical formulae for tensor apparent conductivity of a transversely anisotropic medium, developed for an ideal tensor induction instrument with coinciding positions of all three transmitters and coinciding positions of all three receivers, can be corrected for a practical instrument design. We have introduced the corrected formulae for a practical TIWL instrument. The numerical study shows that, for different relative deviation angles and for different anisotropy values, the corrected apparent conductivities are practically the same as the theoretical apparent parameters. This result indicates that the basic principles of the tensor induction logging developed by Zhdanov et al. (2001a, b) for the ideal tensor instrument under low frequency condition can be easily modified for use with practical tensor instrument data.

ACKNOWLEDGMENTS

The authors acknowledge the support of the University of Utah Consortium for Electromagnetic Modeling and Inversion (CEMI), which includes Baker Atlas Logging Services, BHP Billiton World Exploration Inc., Electromagnetic Instruments, Inc., ExxonMobil Upstream Research Company, INCO Exploration, International Energy Services, Japan National Oil Corporation, MINDECO, Naval Research Laboratory, Rio Tinto-Kennecott, Shell International Exploration and Production Inc., and Sumitomo Metal Mining Co.

The authors are also thankful to Dr. Leo Tabarovsky of Baker Atlas Logging Services and David Kennedy of Exx-

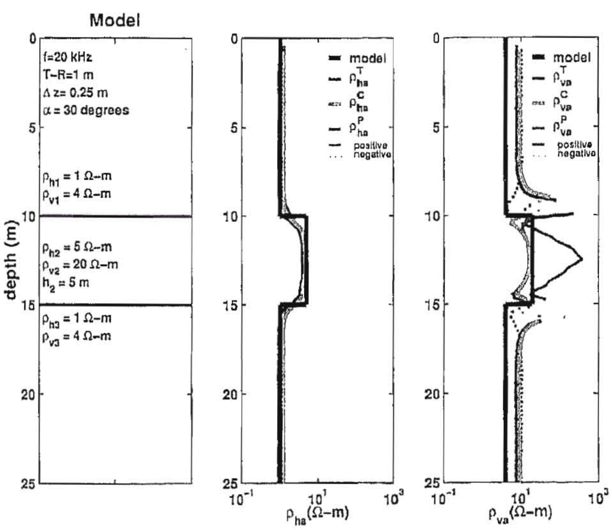

FIG. 6 The first panel on the left shows a three-layer model. The second and the third panels display the horizontal and vertical apparent resistivity curves versus depth, respectively. Solid lines describe the positive values of the apparent resistivities, while the dotted lines correspond to the negative values. The relative deviation angle is 30°. The bold lines represent the apparent resistivities ρ_{ha}^T and ρ_{va}^T obtained by the theoretical formulae for the ideal instrument. The black solid-dotted lines represent the apparent resistivities computed for the practical instrument by the theoretical formulae without correction. The grary solid-dotted lines show the same parameters computed for the practical instrument data after corrections.

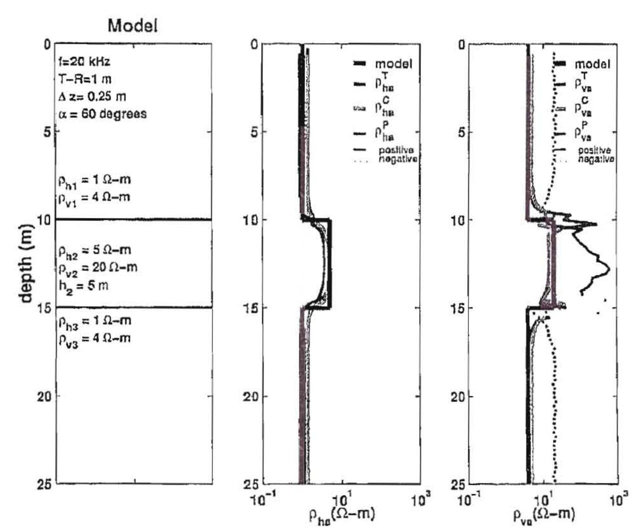

FIG. 7 The first panel on the left shows a three-layer model. The second and the third panels display the horizontal and vertical apparent resistivity curves versus depth, respectively. The relative deviation angle is 60°. The curve's code is the same as in Figure 6.

onMobil Upstream Research Co. for the stimulating discussions which helped to initiate this project.

REFERENCES

Cheryauka, B. A. and Zhdanov, M. S., 2001a, Electromagnetic tensor Green's functions and their integrals in transverse isotropic layered media: Proceedings of the CEMI 2001 Annual Meeting, p. 39–82.

Cheryauka, B. A. and Zhdanov, M. S., 2001b, Fast modeling of a tensor induction tool response in a horizontal well in inhomogeneous anisotropic formations, paper P, *in* 42nd Annual Logging Symposium Transactions: Society of Professional Well Log Analysts.

Cheryauka, B. A. and Zhdanov, M. S., 2001c, Focusing inversion of tensor induction logging data in an anisotropic formation and a deviated well, *in* 71st SEG Annual International Meeting Expanded Abstracts: Society of Exploration Geophysicists, p. 357–360.

Fang, S., and Wang, T., 2000, Accurate Born simulation of induction response using an optimal background, *in* 70th SEG Annual International Meeting Expanded Abstracts: Society of Exploration Geophysicists, p. 1806–1809.

Kriegshauser, B., Fanini, O., Gupta., P., and Yu, L., 2000a, Advanced inversion techniques for multicomponent induction log data, *in* 70th SEG Annual International Meeting Expanded Abstracts: Society of Exploration Geophysicists, p. 1810–1813.

Kriegshauser, B., Fanini, O., Forgang, S., Itskovich, G., Rabinovich, M., Tabarovsky, L., Yu, L, and Epov, M., 2000b, A new multicomponent induction logging tool to resolve anisotropic formation, paper D, *in* 41st Annual Logging Symposium Transactions: Society of Professional Well Log Analysts.

Kriegshauser, B., Fanini, O., Yu, L., Horst, M. and Popta, J., 2001a, Improved shale sand interpretation in highly deviated and horizontal wells using multicomponent induction log data, paper S, *in* 42nd Annual Logging Symposium Transactions: Society of Professional Well Log Analysts.

Kriegshauser, B., McWillams, S., Fanini, O., and Yu, L., 2001b, An efficient and accurate pseudo 2-D inversion scheme for multicomponenet induction log data, *in* 71st SEG Annual International Meeting Expanded Abstracts: Society of Exploration Geophysicists, p. 369–372.

Lu, X. and Alumbaugh, D. L., 2001, One-dimensional inversion of three-component induction logging in anisotropic media, *in* 71st SEG Annual International Meeting Expanded Abstracts: Society of Exploration Geophysicists, p. 376–380.

Martin, L., Chen, D., Hagiwara, T., Strickland, R., Gianzero, S., and Hagan, M., 2001, Neutral network inversion of array induction logging data for dipping beds, paper U, *in* 42nd Annual Logging Symposium Transactions: Society of Professional Well Log Analysts.

Moran, J. H., and Gianzero, S. C., 1979, Effects of formation anisotropy on resistivity logging measurements: *Geophysics*, vol. 44, p. 1266–1286.

Yu, L., Kriegshauser, B., Fanini, O. and Xiao, J., 2001, A fast inversion method for multicomponent induction log data, *in* 71st SEG Annual International Meeting Expanded Abstracts: Society of Exploration Geophysicists, p. 361–64.

Zhang, Z., Yu, L., Krieghauser, B. and Chunduru, R., 2001, Simul-

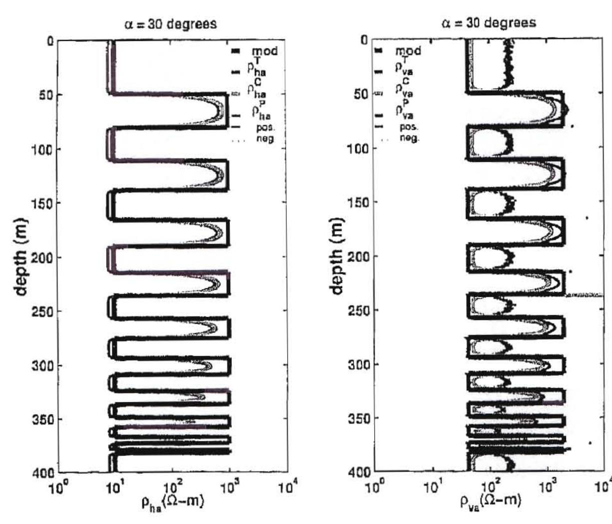

FIG. 8 A generalized chirp type model of anisotropic formation (Fang and Wang, 2000). The left and the right panels display the horizontal and vertical apparent resistivity curves versus depth, respectively. The relative deviation angle is 30°. The curve's code is the same as in Figure 6.

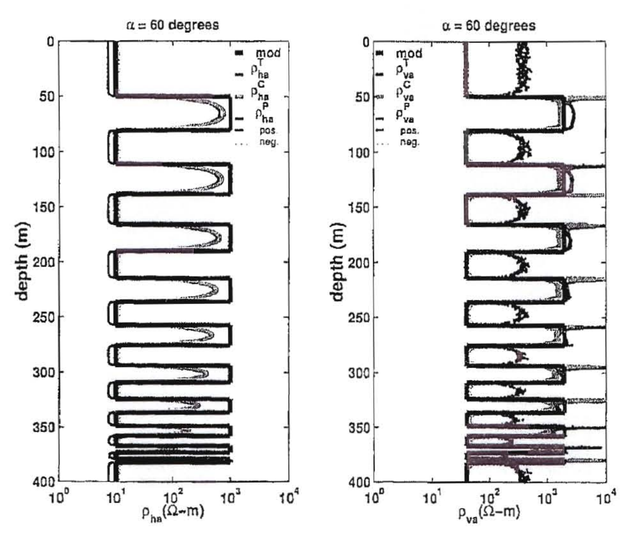

FIG. 9 A generalized chirp type model of anisotropic formation (Fang and Wang, 2000). The left and the right panels display the horizontal and vertical apparent resistivity curves versus depth, respectively. The relative deviation angle is 60°. The curve's code is the same as in Figure 6.

taneous determination of relative angles and anisotropic resistivity using multicomponent induction logging, paper Q, *in* 42nd Annual Logging Symposium Transactions: Society of Professional Well Log Analysts.

Zhang, Z. and Mezzatesta, A., 2001, 2D anisotropic inversion of multicomponent induction logging data, *in* 71st SEG Annual International Meeting Expanded Abstracts: Society of Exploration Geophysicists, p. 365–368.

Zhang, Z., 2001, Recovering absolute formation dip and 1D anisotropic resistivity structure from inversion of multicomponent induction logging data, *in* 71st SEG Annual International Meeting Expanded Abstracts: Society of Exploration Geophysicists, p. 373–375.

Zhdanov, M. S., Kennedy, D., and Peksen, E., 2001a, Foundations of tensor induction well-logging: *Petrophysics*, vol. 42, no. 6, p. 588–610.

Zhdanov, M. S., Kennedy, W. D., Cheryauka, B. A. and Peksen, E., 2001b, Principles of tensor induction well logging in a deviated well in an anisotropic medium, paper R, *in* 42nd Annual Logging Symposium Transactions: Society of Professional Well Log Analysts.

APPENDIX

LOW FREQUENCY APPROXIMATION FOR THE TENSOR INDUCTION MAGNETIC FIELD COMPONENTS

It was demonstrated by Zhdanov et al., (2001a) that the effect of sonde roll can be evaluated from the observations of data in unbounded, homogeneous TI anisotropic medium, so that the rotational angle β can be taken equal to zero. Under this assumption the expressions for low frequency asymptotics of the induction tensor quadrature components in the instrument coordinate frame are

$$\Im H_{x'}^{x'} = g_0\, \sigma_h [1 + 2q\cos^2\alpha], \tag{A.1}$$

$$\Im H_{y'}^{y'} = g_0\, \sigma_h \left[\frac{2}{\lambda\sqrt{\sin^2\alpha + \lambda^2\cos^2\alpha}} - 2q - 1\right], \tag{A.2}$$

$$\Im H_{z'}^{x'} = g_0\, \sigma_h [2q\cos\alpha\sin\alpha] = \Im H_{x'}^{z'}, \tag{A.3}$$

$$\Im H_{z'}^{z'} = g_0\, \sigma_h [2 + 2q\sin^2\alpha], \tag{A.4}$$

$$q = \frac{\lambda\sqrt{\sin^2\alpha + \lambda^2\cos^2\alpha} - \lambda}{\lambda\sin^2\alpha}, \tag{A.5}$$

$\Im$ denotes an imaginary part of the magnetic field component; $H_{x'}^{x'}$, $H_{y'}^{y'}$, $H_{z'}^{z'}$, and $H_{z'}^{x'}$ are the magnetic field components in the instrument coordinate system; g_0 is a parameter,

$$g_0 = \frac{\omega\mu_0}{8\pi L},$$

ω is the angular frequency, μ_0 is the free-space magnetic permeability, $\lambda = \sqrt{\sigma_h / \sigma_v}$ is an anisotropy coefficient, and L is the transmitter-receiver separation.

The analysis of the low frequency asymptotics (A.1)–(A.4) leads to the formulae for the low frequency "horizontal" apparent conductivity, σ_{ha}^T, the apparent anisotropy coefficient, λ_a^T, and the apparent relative deviation angle, α_a^T, given by (Zhdanov et al. 2001a, b),

$$\sigma_{ha}^T = \frac{1}{2g_0}\left[\Im H_{x'}^{x'} + \frac{1}{2}\Im H_{z'}^{z'} + \sqrt{\left(\Im H_{x'}^{x'} - \frac{1}{2}\Im H_{z'}^{z'}\right)^2 + 2\Im^2 H_{z'}^{x'}}\right], \tag{A.6}$$

$$\lambda_a^T = \frac{4g_0^2\left(\sigma_{ha}^T\right)^2}{\Im H_{z'}^{z'}\left(\Im H_{y'}^{y'} + \Im H_{x'}^{x'} + \Im H_{z'}^{z'} - 2g_0\sigma_{ha}^T\right)}, \tag{A.7}$$

$$\alpha_a^T = \frac{1}{2}\sin^{-1}\left[\frac{2\Im H_{z'}^{x'}}{\Im H_{x'}^{x'} + \Im H_{z'}^{z'} - 3g_0\sigma_{ha}^T}\right], \tag{A.8}$$

where superscript T indicates that these are the theoretical parameters computed for the "ideal instrument."

The expression for the "vertical" apparent conductivity, σ_{va}^T is

$$\sigma_{va}^T = \frac{\sigma_{ha}^T}{(\lambda_a^T)^2}. \tag{A.9}$$

Thus, the TIWL method consists in measuring the components of the magnetic induction tensor using a tri-axial induction instrument and computing the apparent conductivities using formulae (A.6) and (A.9).

ABOUT THE AUTHORS

Michael S. Zhdanov is Professor of Geophysics, Director of the Consortium for Electromagnetic Modeling and Inversion (CEMI) at the University of Utah since 1993. He received his PhD in physics and mathematics in 1970 from Moscow State University. He was previously the Director of the Geoelectromagnetic Research Institute of the Russian Academy of Sciences, Moscow.

Dr. Zhdanov is Honorary Gauss Professor, Gettingen Academy of Sciences, Germany, Full Member of Russian Academy of Natural Sciences, Honorary Professor of China National Center of Geological Exploration Technology, and Member of the Electromagnetics Academy, USA.

His main research interest is developing methods for the solution of forward and inverse problems in geophysics, new techniques for electromagnetic imaging of the earth's interior. He is the author of several books on geophysical electromagnetic theory and inverse problem solutions.

Ertan Peksen is a PhD student at the Consortium for Electromagnetic Modeling and Inversion (CEMI), the University of Utah.

He graduated in 1993 (BS) from the University of Ankara, in geophysics. He received his Master of Science degree in geophysics from the Department of Geology and Geophysics, University of Utah, in 1999.

His research interest is modeling and inversion of tensor induction well logging data in anisotropic media.